

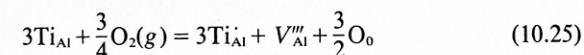
Fig. 10.23. Effect of particle size on the contact area growth in  $\text{Al}_2\text{O}_3$  heated 100 hr at  $1600^\circ\text{C}$ . From R. L. Coble.

The other variable appearing in Eqs. 10.22 and 10.24 that is subject to analysis and some control is the diffusion coefficient; it is affected by composition and by temperature; the relative effectiveness of surfaces, boundaries, and volume as diffusion paths is affected by the microstructure. A number of relationships similar to Eqs. 10.23 and 10.24 have been derived, and it has been shown that surface diffusion is most important during early stages of sintering (these affect the neck diameter between particles but not the shrinkage or porosity); grain-boundary diffusion and volume diffusion subsequently become more important. In ionic ceramics, as discussed in Chapter 9, both the anion and the cation diffusion coefficients must be considered. In  $\text{Al}_2\text{O}_3$ , the best studied material, oxygen diffuses rapidly along the grain boundaries, and the more slowly moving aluminum ion at the boundary or in the bulk controls the overall sintering rate. As discussed in Chapter 5, the grain-boundary structure, composition, and electrostatic charge are influenced strongly by temperature and by impurity solutes; as discussed in Chapter 6, the exact mechanism of grain-boundary diffusion remains controversial. Estimates of the grain-boundary-diffusion width from sintering data range from 50 to 600 Å. These complications require us to be careful not to overanalyze data in terms of specific numerical results, since the time or temperature dependence of sintering may be in accordance with several plausible models. In general the presence of solutes which enhance either

boundary or volume diffusion coefficients enhance the rate of solid-state sintering. As discussed in Chapter 6, both boundary and volume diffusion coefficients are strongly temperature-dependent, which means that the sintering rate is strongly dependent on the temperature level.

In order to effectively control sintering processes which take place by solid-state processes, it is essential to maintain close control of the initial particle size and particle-size distribution of the material, the sintering temperature, the composition and frequently the sintering atmosphere.

As an example of the influence of solutes, Fig. 10.24 illustrates the effect of titania additions on the sintering rate of a relatively pure alumina in a region of volume diffusion. (Both volume and boundary diffusion processes are enhanced.) It is believed that Ti enters  $\text{Al}_2\text{O}_3$  substitutionally as  $\text{Ti}^{+3}$  and  $\text{Ti}^{+4}$  ( $\text{Ti}_{\text{Al}}$  and  $\text{Ti}_{\text{Al}}''$ ). At equilibrium



from which 
$$K_1 = \frac{[\text{Ti}_{\text{Al}}']^3 [V_{\text{Al}}''']}{[\text{Ti}_{\text{Al}}]^3 [P_{\text{O}_2}]^{3/4}} \quad (10.26)$$

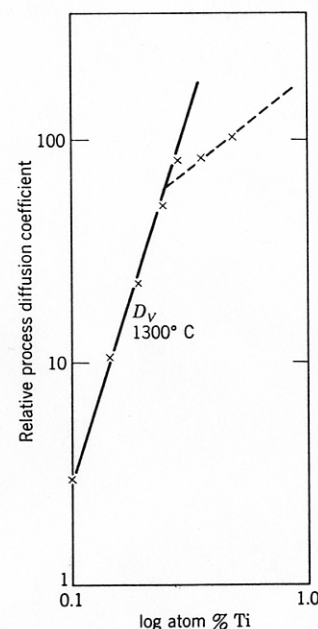


Fig. 10.24. Data for the relative sintering process diffusion coefficient with Ti additions to  $\text{Al}_2\text{O}_3$ .  $D_\alpha[\text{Ti}]^3$ . From R. D. Bagley, I. B. Cutler, and D. L. Johnson, *J. Am. Ceram. Soc.*, 53, 136 (1970); R. J. Brook, *J. Am. Ceram. Soc.*, 55, 114 (1972).

In the powders used, divalent impurities such as magnesium exceed in concentrations the intrinsic defect levels, so that overall charge neutrality at moderate titania levels is achieved by

$$[\text{Ti}_{\text{Al}}] = [\text{Mg}'_{\text{Al}}] \quad (10.27)$$

and at constant impurity and oxygen pressure levels, combining Eqs. 10.26 and 10.27 gives

$$[V''_{\text{Al}}] = K_2[\text{Ti}_{\text{Al}}]^3 \quad (10.28)$$

Since the total Ti addition ( $\text{Ti}_{\text{Al}} + \text{Ti}'_{\text{Al}}$ ) is much greater than the impurity levels,  $[\text{Ti}]_{\text{Total}} \approx [\text{Ti}_{\text{Al}}]$  and  $[V''_{\text{Al}}] \approx K_2[\text{Ti}]_{\text{Total}}^3$ . The dependence of lattice defect concentrations on titania concentration is shown in Fig. 10.25 for the proposed model. As discussed in Chapter 6, the diffusion coefficient is proportional to the vacancy concentration; as a result the effect of this model is to anticipate an increase in the sintering rate proportional to the third power of titania concentration as experimentally observed (Fig. 10.24). At higher concentrations the dependence on titania concentration should become less steep, which is suggested by the sintering data.

Thus far our discussion of the variables influencing the sintering process has been based on the initial stages of the process, in which models are based on solid particles in contact. As the process continues, an intermediate microstructure forms in which the pores and solid are both continuous, followed by a later stage in which isolated pores are separated from one another. A number of analytical expressions have

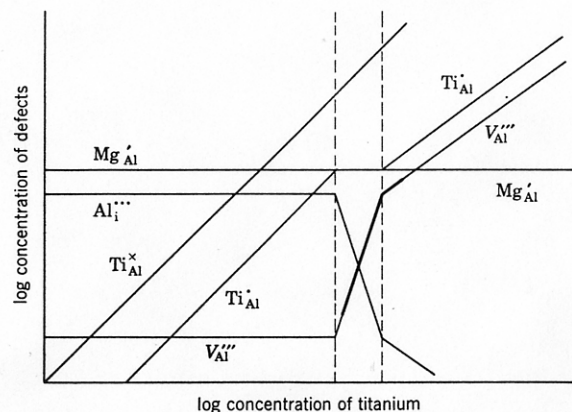


Fig. 10.25. Model for the dependence of defect concentrations on the Ti concentration in  $\text{Al}_2\text{O}_3$ . From R. J. Brook, *J. Am. Ceram. Soc.*, 55, 114 (1972).

been derived from specific microstructural models for the transport processes listed in Table 10.1. In the later stages of the process only two mechanisms are important: boundary diffusion from sources on the boundary and lattice diffusion from sources on the boundary. For a nearly spherical pore the flux of material to a pore can be approximated as

$$J = 4\pi D_v \Delta c \left( \frac{rR}{R-r} \right) \quad (10.29)$$

where  $D_v$  is the volume diffusion coefficient,  $\Delta c$  is the excess vacancy concentration (Eq. 10.21),  $r$  is the pore radius, and  $R$  is the effective-material-source radius. The importance of microstructure in applying this sort of analysis to specific systems is illustrated in Fig. 10.26. For a sample

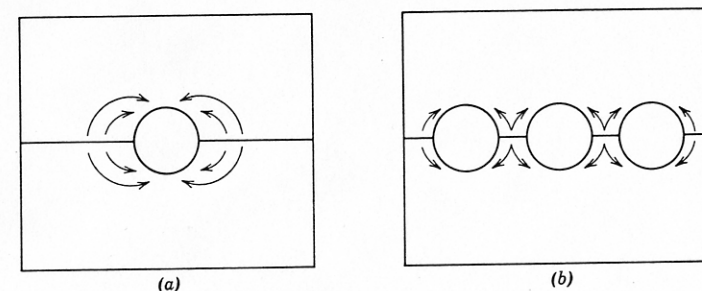


Fig. 10.26. The mean diffusion distance for material transport is smaller when there are more of the same size of pores in a boundary.

with a larger number of pores, all the same size, on a boundary the mean diffusion distance is smaller when there are more pores, and pore elimination is accomplished more quickly for the sample with the higher porosity. Thus, although the terms which influence the rate of sintering—volume or boundary diffusion coefficient (and therefore temperature and solute concentration) surface energy and pore size—are well established, the geometrical relationship of grain boundaries to the pores may have a variety of forms and is critical in determining what actually occurs.

With fine-grained materials such as oxides, it is usual to observe an increase in both grain size and pore size during the early stages of heat treatment, as illustrated for Lucalox alumina in Fig. 10.27. This partially results from the presence of agglomerates of the fine particles which sinter rapidly, leaving interagglomerate pores, and is partly due to the rapid grain growth during which pores are agglomerated by moving with the boundaries, as illustrated in Fig. 10.9. In cases in which agglomeration



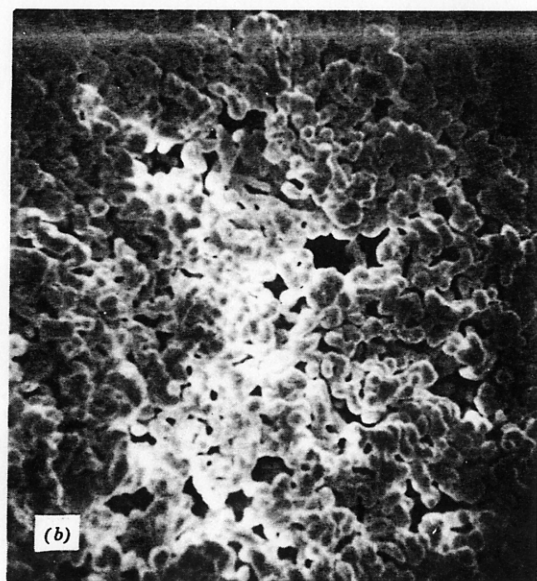
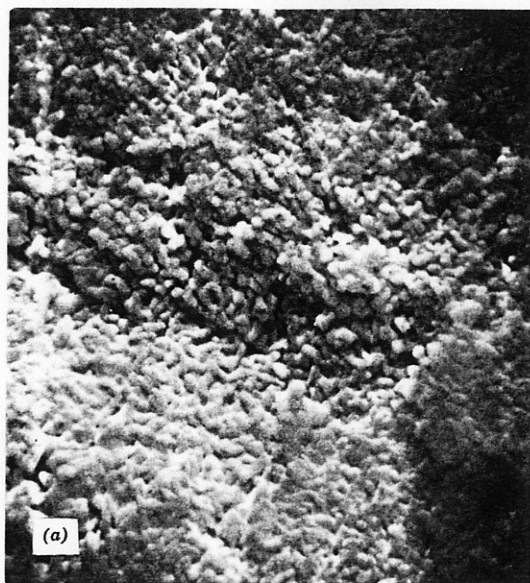


Fig. 10.27. Progressive development of microstructure in Lucalox alumina. Scanning electron micrographs of (a) initial particles in the compact (5000 $\times$ ), (b) after 1 min at 1700°C (5000 $\times$ ).

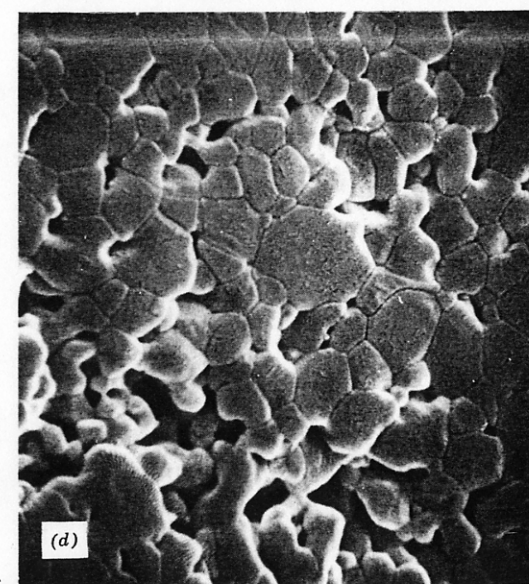
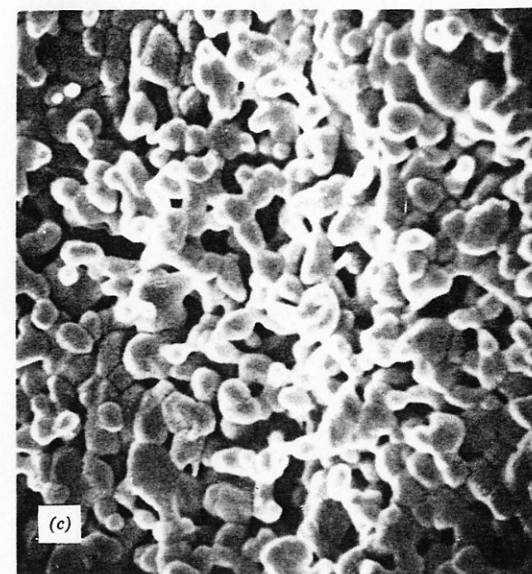


Fig. 10.27 (Continued) (c) Scanning electron micrographs after 2½ min at 1700°C (5000 $\times$ ), and (d) after 6 min at 1700°C (5000 $\times$ ). Note that pores and grains increase in size, that there are variations in packing and in pore size, and that pores remain located between dense grains.

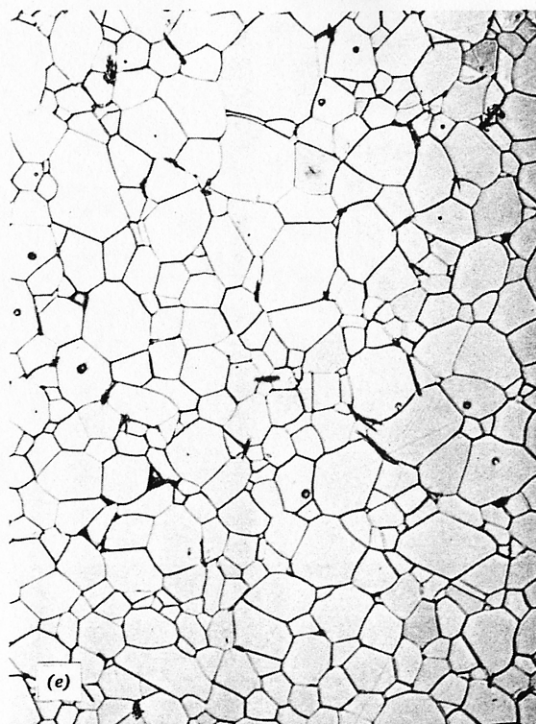


Fig. 10.27 (Continued) (e) The final microstructure is nearly porefree, with only a few pores located within grains (500 $\times$ ). Courtesy C. Greskovich and K. W. Lay.

of fine precipitated particles into clumps is severe, ball milling to break up the agglomerates leads to a remarkable increase in the sintering rate. Even minor variations in the original particle packing are exaggerated during the pore growth process; in addition, spaces between agglomerates and occasional larger voids resulting from the bridging of particles or agglomerates are present. As a result, during intermediate stages of the sintering process there is a range of pore sizes present, and the slower elimination of the larger pores leads to variations in pore concentration in the later stages of the sintering process, as illustrated in Fig. 10.28c.

In addition to local agglomerates and packing differences, pore-concentration variations in the later stages of sintering can result from particle-size variations in the starting material, from green density varia-

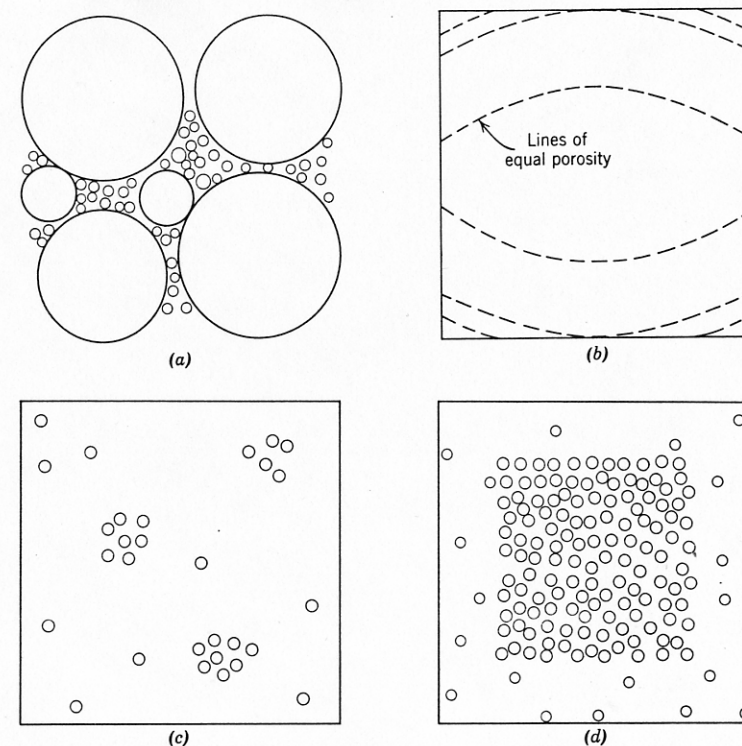


Fig. 10.28. Pore-concentration variations resulting from (a) a variation in grain sizes, (b) die friction, (c) local packing and agglomeration differences, and (d) more rapid pore elimination near surfaces.

tions caused by die-wall friction during pressing, and from the more rapid elimination of porosity near surfaces caused by temperature gradients during heating, as shown in Fig. 10.28. The importance of local variations in pore concentration results from the fact that the part of the sample containing pores tends to shrink but is restrained by other porefree parts. That is, the effective diffusion distance is no longer from the pore to an adjacent grain boundary but a pore-pore or pore-surface distance many orders of magnitude larger. An example of residual pore clusters in a sintered oxide is shown in Fig. 10.29.

Not only the kinetics of pore elimination can lead to "stable" and residual porosity, but it is also possible in some cases to have a thermodynamically metastable equilibrium pore configuration. In Fig.



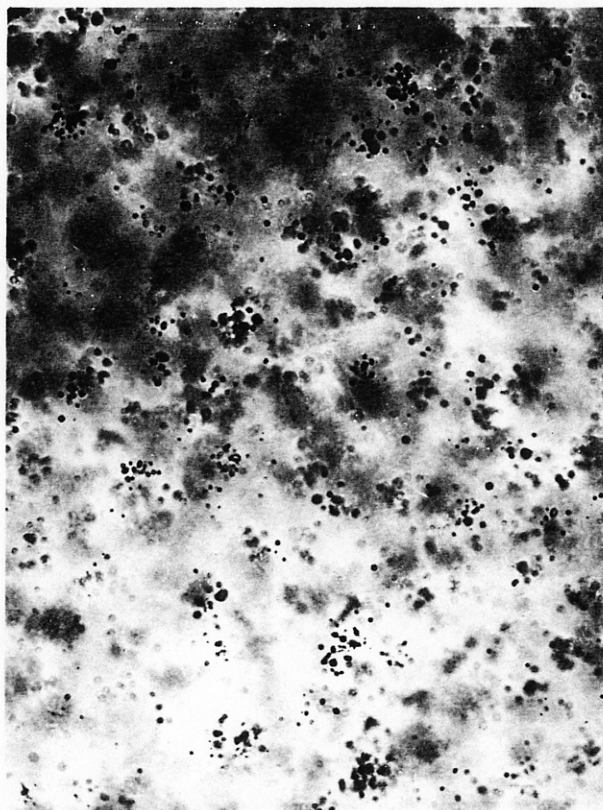


Fig. 10.29. Residual pore clusters resulting from improper powder processing in a sample of 90 mole %  $\text{Y}_2\text{O}_3$ -10 mole %  $\text{ThO}_2$ . Transmitted light, 137 $\times$ . Courtesy C. Greskovich and K. N. Woods.

10.26 we have drawn spherical pores located on a grain boundary, the usual model description, but we know from our discussion of interface energies in Chapter 5 that there is a dihedral angle  $\phi$  at the pore-boundary intersection determined by the relative interface energies;

$$\cos \frac{\phi}{2} = \frac{\gamma_{gb}}{2\gamma_s} \quad (10.30)$$

In most cases the dihedral angle for pure oxides is about  $150^\circ$ , and the spherical pore approximation is quite good; but for  $\text{Al}_2\text{O}_3 + 0.1\% \text{MgO}$  the

value is  $130^\circ$ , for  $\text{UO}_2 + 30 \text{ ppm C}$  the value is  $88^\circ$ , and for impure boron carbide the value is about  $60^\circ$ . For these materials the consequences of nonspherical pores have to be considered.

As discussed for discontinuous grain growth and illustrated in Figs. 10.4 and 10.11, the boundary curvature between grains or phases depends both on the value of the dihedral angle and on the number of surrounding grains. If we take  $r$  as the radius of a circumscribed sphere around a polyhedral pore surrounded by grains, the ratio of the radius of curvature of the pore surfaces  $\rho$  to the spherical radius depends both on the dihedral angle and on the number of surrounding grains, as shown in Fig. 10.30a. When  $r/\rho$  decreases to zero, the interfaces are flat and have no tendency

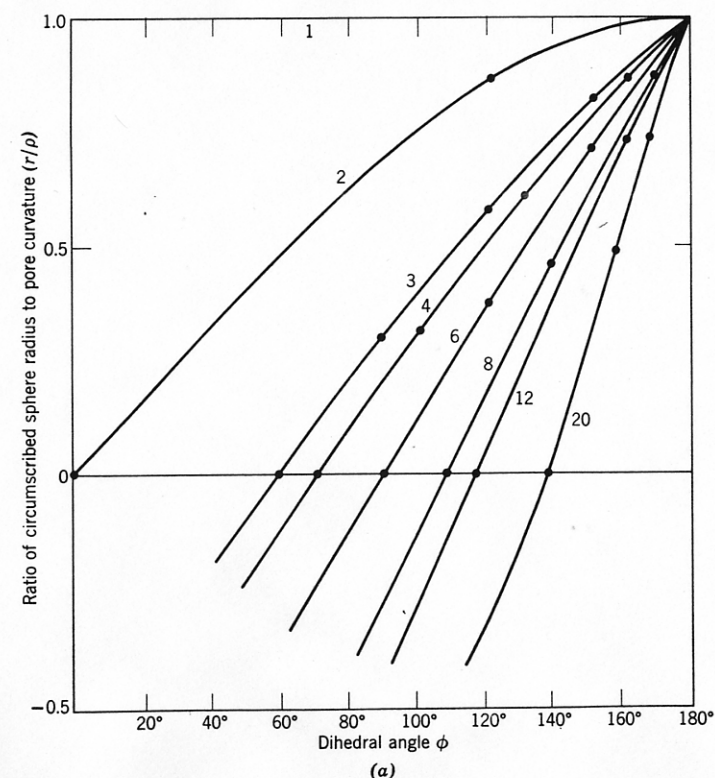


Fig. 10.30. (a) Change in the ratio  $(r/\rho)$  with dihedral angle for pores surrounded by different numbers of grains as indicated on individual curves.